Journal of Magnetic Resonance 200 (2009) 285–290

Contents lists available at ScienceDirect

Journal of Magnetic Resonance

journal homepage: www.elsevier.com/locate/jmr

Distortion-free magnetic resonance imaging in the zero-field limit

Nathan Kelso [a,c], Seung-Kyun Lee [a,c,1], Louis-S. Bouchard [b,c,2], Vasiliki Demas [b,c,3], Michael Mück [d], Alexander Pines [b,c], John Clarke [a,c,*]

[a] Department of Physics, University of California, Berkeley, CA 94720, USA
[b] Department of Chemistry, University of California, Berkeley, CA 94720, USA
[c] Materials Sciences Division, Lawrence Berkeley National Laboratory, Berkeley, CA 94720, USA
[d] Institut für Angewandte Physik, Justus-Leibig-Universität Gießen, D-35392 Gießen, Germany

ARTICLE INFO

Article history:
Received 9 July 2009
Available online 18 July 2009

Keywords:
Low-field MRI
Concomitant gradients
Image distortion
Mobile NMR
SQUID-detected NMR
Coherent averaging

ABSTRACT

MRI is a powerful technique for clinical diagnosis and materials characterization. Images are acquired in a homogeneous static magnetic field much higher than the fields generated across the field of view by the spatially encoding field gradients. Without such a high field, the concomitant components of the field gradient dictated by Maxwell's equations lead to severe distortions that make imaging impossible with conventional MRI encoding. In this paper, we present a distortion-free image of a phantom acquired with a fundamentally different methodology in which the applied static field approaches zero. Our technique involves encoding with pulses of uniform and gradient field, and acquiring the magnetic field signals with a SQUID. The method can be extended to weak ambient fields, potentially enabling imaging in the Earth's field without cancellation coils or shielding. Other potential applications include quantum information processing and fundamental studies of long-range ferromagnetic interactions.

1. Introduction

In MRI, the Larmor precession frequency $\omega(x, y, z) = \gamma B(x, y, z)$ of the proton spins in the position-dependent magnetic field $B(x, y, z)$ frequency- and phase-encodes the proton density distribution into a magnetic signal that is subsequently decoded to form an image [1] (γ is the magnetogyric ratio). In clinical MRI machines [1] the strength of the applied homogeneous static magnetic field $\boldsymbol{B_0} = B_0\,\hat{z}$ is typically 1.5 T. There has been recent interest, however, in systems operating in magnetic fields of the order of 10^{-4} T (for example [2–7]), where T_1-weighted contrast is significantly enhanced [5] (T_1 is the longitudinal relaxation time). The loss of polarization is compensated—at least in part—by prepolarizing [8] the spins at a much higher field, or by hyperpolarization techniques using lasers [9], dynamic nuclear polarization [10,11] or parahydrogen-induced polarization [12]. As the frequency is lowered, the loss of signal amplitude inherent in Faraday-Law detection is mitigated by detecting the nuclear magnetization with either a Superconducting QUantum Interference Device (SQUID) [13] or an atomic magnetometer [14], both of which respond to the magnetic flux itself, rather than its time rate of change. Regardless of the magnitude of B_0, all currently used imaging processes involve the superposition of magnetic field gradients on a static field to impose spatial variations of the total field across the subject or sample. In the zero static field regime reported here, conventional MRI gradients are unable to encode the spins along a given direction and Fourier encoding breaks down.

2. Theory

In conventional MRI techniques, the applied magnetic field gradients are assumed to be linear and unidirectional so that the field due to gradients is given by $\boldsymbol{B}(x, y, z) = (G_x x + G_y y + G_z z)\,\hat{z}$, where $G_x = \partial B_z/\partial x$, $G_y = \partial B_z/\partial y$, and $G_z = \partial B_z/\partial z$ are constants [1]. As an example, $\boldsymbol{B}(x, y, z) = G_z z\,\hat{z}$ is shown in Fig. 1a. In reality, however, such idealized gradients are forbidden by the Maxwell equations $\mathrm{div}\boldsymbol{B} = \mathrm{curl}\boldsymbol{B} = 0$ for any time-independent magnetic field $\boldsymbol{B}$ in free space. In fact, any gradient must be accompanied by concomitant gradients in at least one additional direction, as illustrated in Fig. 1b. At very low static fields the undesired gradient components perpendicular to $\boldsymbol{B_0}$ induce severe image distortions [15–17]. The degree of distortion is characterized by a parameter $\varepsilon = GL/B_0$, where G is the magnitude of the field gradient and L is the image field of view (FOV) [17]. When $\varepsilon \ll 1$, the gradient fields can be approximated as unidirectional, greatly simplifying image encoding and reconstruction and leading to negligible image distortion.

* Corresponding author. Address: Department of Physics, University of California, 366 LeConte Hall #7300, Berkeley, CA, 94720-7300, USA. Fax: +1 510 642 1304.
E-mail address: jclarke@berkeley.edu (J. Clarke).
[1] Present address: GE Global Research, One Research Circle, Niskayuna, NY 12309, USA.
[2] Present address: Department of Chemistry and Biochemistry, 607 Charles E. Young Dr. East, University of California, Los Angeles, CA 90095, USA.
[3] Present address: T2 Biosystems, 286 Cardinal Medeiros Ave., Cambridge, MA 02141, USA.

1090-7807/$ - see front matter © 2009 Elsevier Inc. All rights reserved.
doi:10.1016/j.jmr.2009.07.016

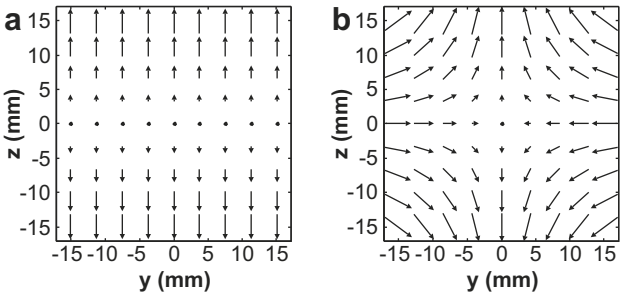

Fig. 1. Idealized and achievable magnetic field gradients. (a) Idealized gradient field $\boldsymbol{B} = (\partial B_z/\partial z)z\,\hat{z}$. Such a field violates Maxwell's equations. (b) Example of a realizable gradient field in the y–z plane of the form $\boldsymbol{B}(y, z) = (\partial B_y/\partial y)y\,\hat{y} + (\partial B_z/\partial z)z\,\hat{z}$. Lengths of vectors represent relative field strengths.

This "truncation" of the concomitant fields forms the basis of nearly all MRI techniques used today including projection reconstruction and Fourier imaging [1].

Several approaches have been proposed for imaging in the regime $\varepsilon >> 1$ where conventional techniques fail [18–20]. Our experiment relies on the fact that, for very small angles, the precession of spins about an arbitrary field $\boldsymbol{B}$ can be represented by the sum of the precessions about each component of $\boldsymbol{B}$ [18]. After such a precession, the magnetization components that have evolved in the concomitant field can be reversed while leaving the desired unidirectional encoded component unchanged, an example of an average Hamiltonian [21]. Fig. 2a shows the pulse sequence for two-dimensional imaging in the limit of zero static field, and Fig. 2b and c depicts the classical evolution of spins at (y', z') subjected to this sequence. The proton spins are first polarized along the x-axis by a large field B_p which is turned off nonadiabatically [11] at time $t = 0$ (point A in Fig. 2a–c). The gradient field with the approximate form (cross terms have been neglected)

$$\boldsymbol{B}(y,z) = (\partial B_y/\partial y)y\,\hat{y} + (\partial B_z/\partial z)z\,\hat{z} \tag{1}$$

is turned on, and subsequently turned off nonadiabatically at time τ (point B). During this time interval, the spin precesses about $\boldsymbol{B}(y', z')$. The time τ is chosen to satisfy the requirement $\tau << 1/\gamma G_z L$. Consequently, the precession during the interval τ is small, and we can treat it as the sum of precessions around $\hat{z}$ and $\hat{y}$: $\delta_z = \gamma(\partial B_z/\partial z)z'\tau$ around $\hat{z}$ (Fig. 2b) and $\delta_y = \gamma(\partial B_y/\partial y)y'\tau$ around $\hat{y}$ (Fig. 2c). After the gradient pulse, a π pulse of uniform field B_π is applied along the z-axis with amplitude and duration adjusted to produce a precession angle of π around $\hat{z}$. This pulse flips the spin to the point C in Fig. 2b and c. Subsequently, a second gradient pulse brings the spin to D, and a second π pulse to E. This sequence of pulses produces a net precession of the spin about B_z, but no net precession about B_y. Thus, the two π pulses average out the components of field perpendicular to $\hat{z}$, leaving an effectively unidirectional gradient field $\boldsymbol{B}_{\mathbf{eff}}(y, z) = G_z z\,\hat{z}$.

To implement this sequence, it is convenient to define a "pulse unit" consisting of two gradient pulses and two π pulses. Clearly, the addition of subsequent pulse units increases the angle of precession about $\hat{z}$. After n pulse units, the gradient has been applied for a total time $t_n = 2n\tau$. Data are acquired at discrete values of k, namely

$$k(t_n) = \gamma \int_0^{t_n} G_z(t)dt, \tag{2}$$

using point-by-point detection in which each point in k-space is acquired in a separate experiment. After the final pulse unit, a small measurement field B_m is turned on along the z-axis and the NMR signal from precession about this field is detected (Fig. 2d). The Fourier transform of this real-valued signal produces a complex-valued

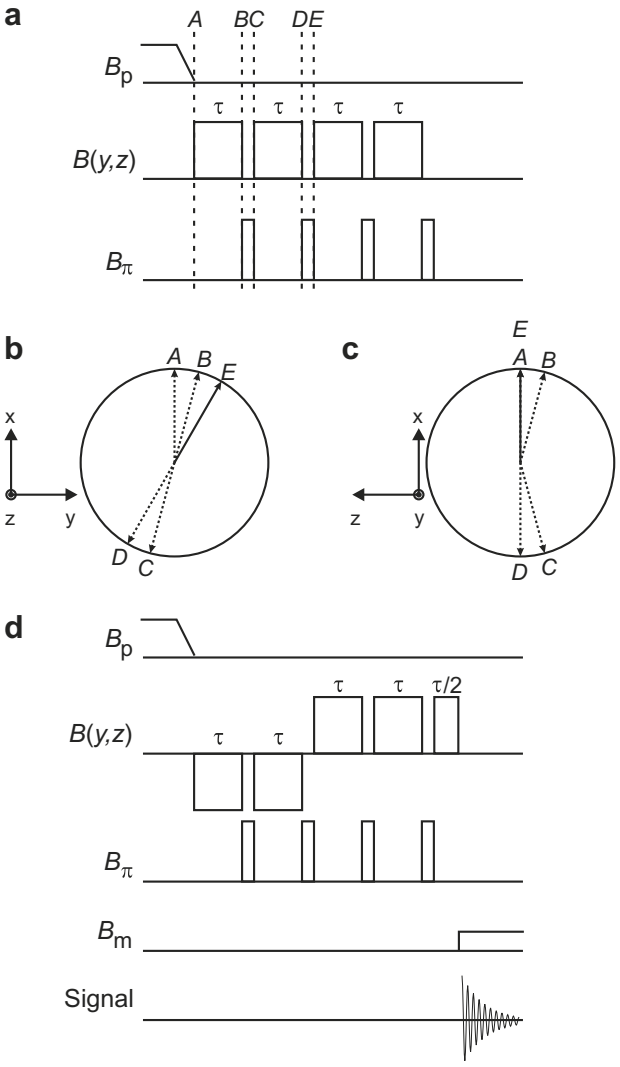

Fig. 2. Protocol for MRI in zero static field. (a) Pulse sequence vs. time. (b and c) Progression of the spin vector at times $t = 0$ (A), τ (B), 2τ (C), 3τ (D) and 4τ (E) about (b) z-axis and (c) y-axis. (d) Pulse sequence used for the zero-field MRI experiment differs from that in b in two respects. First, after the final pulse pair, a gradient pulse was applied for a time $\tau/2$; this pulse corrects higher order errors [18,19]. Second, to ensure that the important $k = 0$ point was included, the gradient was inverted in the first pulse unit, so that the first point in k-space was $k(5\tau/2) = -(3\tau/2)\gamma G_z$. All subsequent gradient pulses have positive polarity; for example, the second k-space point was $k(9\tau/2) = (\tau/2)\gamma G_z$. Note that the measurement field B_m is *not* applied during encoding pulses; it is used solely for point-by-point k-space acquisition, enabling quadrature detection with a single sensor.

peak in frequency space, yielding the real and imaginary parts of the signal at $k(2n\tau)$. After completing the acquisition, the k-space projection is Fourier transformed to obtain a one-dimensional, real-space projection of the sample. Subsequently, we rotate the sample through an angle θ ($<<\pi$) and acquire another projection; the procedure is repeated until the range from 0° to 180° is covered. The image is reconstructed using filtered back-projection [1].

3. Experimental methods

The experimental configuration is shown schematically in Fig. 3. A double-walled Pyrex vacuum vessel is immersed in liquid helium contained in a dewar surrounded with a single-layer mu-metal shield to attenuate external magnetic fields. A superconducting lead shield inside the dewar stabilizes the residual magnetic